Materials Characterization 134 (2017) 246–252

Contents lists available at ScienceDirect

Materials Characterization

journal homepage: www.elsevier.com/locate/matchar

Microstructure evolution and mechanical performance of copper processed by equal channel angular rolling

T. Kvackaj[a], A. Kovacova[a], R. Kocisko[a], J. Bidulska[a], L. Lityńska–Dobrzyńska[b], P. Jenei[c], J. Gubicza[c,*]

[a] Faculty of Metallurgy, Technical University of Košice, Letna 9, 04200 Kosice, Slovakia
[b] Institute of Metallurgy and Materials Science of the Polish Academy of Science, Krakow, Poland
[c] Department of Materials Physics, ELTE Eötvös Loránd University, Budapest, Hungary

ARTICLE INFO

Keywords:
Equal channel angular rolling (ECAR)
Ultrafine-grained copper
Microstructure
Dislocation density
Mechanical properties

ABSTRACT

Ultrafine-grained (UFG) oxygen free high conductivity (OFHC) Cu samples were processed by severe plastic deformation (SPD) using the method of equal channel angular rolling (ECAR) up to 33 passes at room temperature. It was found that the grain size gradually decreased from ~40 μm to ~250 nm with increasing the number of passes. A maximum dislocation density of ~21 × 10^{14} m^{-2} was achieved after 13 passes of ECAR. For large numbers of passes (between 23 and 33), the dislocation density decreased to ~14 × 10^{14} m^{-2}. The proof stress was saturated at the value of about 400 MPa. The stored energy was measured by calorimetry and compared with the values calculated from the parameters of the microstructure. The reduction of the released heat after 13 and 33 passes suggested structural relaxation of the UFG microstructure. For these numbers of passes, the reduction of area in tensile testing was improved without decreasing the proof stress. The correlation between the microstructure and the mechanical behavior was discussed in detail. It was found that ECAR is capable for the mass-production of UFG metallic materials with high strength, therefore this method is a possible way of commercialization of SPD-processed materials.

1. Introduction

Porosity and contamination-free, high strength metallic materials can be produced by severe plastic deformation (SPD) procedures [1–3]. Applying these methods, the elevated mechanical strength is achieved via the refinement of the grain structure into the ultrafine-grained (UFG) regime and the increase of the dislocation density to extremely high values [4]. Numerous SPD procedures were developed in the last decades, such as equal channel angular pressing (ECAP) [5–8], high-pressure torsion (HPT) [9], multi-directional forging (MDF) [10], twist extrusion (TE) [3,11] and accumulative roll-bonding (ARB) [3]. Although, these methods yield UFG metallic materials with high strength, they are not suitable for mass-production due to the very limited dimensions of the as-processed workpieces.

Efforts were made in the literature to develop SPD procedures which are capable to process large amounts of UFG materials in a reasonable time. For instance, the classical ECAP technique was modified in order to provide a solution for the continuous production of UFG materials which is referred to as ECAP-Conform process [5]. Another candidate for mass-production of UFG metals is equal channel angular rolling (ECAR) which combines rolling and ECAP steps in materials processing [12]. First, the workpiece is rolled and then the specimen passed between the rolls is introduced into an ECAP die. This process can be carried out either on large, thin sheets or long, rod-like samples. In the last decade, ECAR-processing was successfully applied on pure Cu [13,14], Al-alloys such as Al 5083 [15], Al 1100 [16], Al 7050 [17], Mg-alloys such as AZ31 [18–20] and bimetal Al/Cu sheets [21]. It was shown that ECAR resulted in a significant grain refinement for all metallic materials. For instance, in AZ31 alloys the initial grain size of ~20 μm was reduced to about 30 nm after 10 passes of ECAR [20]. The significant grain refinement yielded a considerable increase in strength and hardness. It seems that the majority of grain refinement and hardness increment occurred during the first pass of ECAR [16]. The ductility usually decreases for ECAR-processed materials due to the loss of the strain hardening capability [15]. At the same time, for AZ31 alloy the drawability was improved by ECAR owing to the variation of the deformation mechanisms as a result of the change in the crystallographic texture [18,19]. For precipitation-hardened Al-alloys, ECAR-processing led to a fragmentation of plate-like precipitates into spherical particles which also influences the hardness [17]. It was shown

* Corresponding author.
E-mail address: jeno.gubicza@ttk.elte.hu (J. Gubicza).

http://dx.doi.org/10.1016/j.matchar.2017.10.030
Received 28 August 2017; Received in revised form 30 October 2017; Accepted 30 October 2017
Available online 31 October 2017
1044-5803/

that ECAR-processing of Cu strips at room temperature (RT) led to a high strength of about 300 MPa and a reduced elongation to failure (about 6%) [14]. In that work, the maximum number of passes was eight. It was also revealed that short time annealing after ECAR-processing may yield a slight improvement in strength, ductility and conductivity due to partial recrystallization. Other work [13] has shown that the application of ECAR on a Cu bar with rectangular cross section can yield a very large strength of about 400 MPa. In these experiments, ECAR deformation was performed only up to 13 passes.

The goal of this study is to investigate the microstructure, the thermal stability and the mechanical behavior of ECAR-processed Cu. The results obtained on the specimens processed by ECAR are compared with the properties of ECAP-processed Cu samples as ECAR is suitable for mass production while ECAP is mainly a laboratory technique. Former studies on ECAP-processed Cu have shown that deformation up to very high numbers of passes (16–25 passes [22,23]) can result in a structural relaxation which may improve the ductility of the UFG Cu specimens. Similar study on ECAR-processed Cu is missing from the literature. Therefore, the present study was extended to 33 passes of ECAR. The microstructure was studied by transmission electron microscopy (TEM) and X-ray line profile analysis (XLPA). The latter method enables the determination of the density and arrangement of dislocations with good statistics. Our study is unique in the literature as the dislocation structure in ECAR-processed Cu has not been studied yet. In addition, the energy stored in the lattice defect structure was determined by calorimetry as a function of the number of passes. The correlation between the mechanical performance and the microstructure was discussed in detail.

2. Experimental Material and Methods

The initial material was oxygen free high conductivity copper (OFHC with the purity of 99.99%). The grain size and the mechanical properties of the initial OFHC Cu are given in Table 1. The initial Cu samples were processed by zonal refining and cold drawing with an elongation of 200%. Then, the specimens were subjected to one pass of caliber rolling before their entering the ECAR channel. The schematic of the ECAR facility is shown in Fig. 1. Specimens were processed by ECAR with a die channel angle of $\Phi = 90^{\circ}$ at RT. Before ECAR, the samples have a rectangular cross section with the dimension of 7×6 mm^2 and a length of 500 mm. The ECAR process was carried out using a duo rolling mill with rolls diameter of D = 210 mm. The pressing velocity during ECAR was 0.2 mm/s. Route A was applied, i.e., the samples were not rotated between the subsequent passes. The maximum number of ECAR passes was 33. Finite element modeling (not shown here) revealed that the temperature of the specimens during ECAR increased to about 90 °C. The microstructure and the mechanical behavior were studied as a function of the numbers of ECAR passes. The microstructure was investigated by TEM using a Philips CM20 microscope. The surface of the TEM foil was parallel to plane *x-z* shown in Fig. 1. It is noted that in order to avoid any recovery and recrystallization during the study of the severely deformed microstructures, the ECAR-processed samples were stored in a freezer.

The microstructure of the specimens was also studied by XLPA. The X-ray line profiles were measured by a high-resolution rotating anode diffractometer (Rigaku, RA Multimax9) using CuKα_1 ($\lambda = 0.15406$ nm)

Table 1
The grain size and the mechanical properties of the initial OFHC Cu. d is the grain size, $R_{p0.2}$ is the proof stress at the strain of 0.2%, R_m is the tensile strength, A_5 is the elongation to failure and *Z* is the reduction in area during tension.

d [μm]	$R_{p0.2}$ [MPa]	R_m [MPa]	A_5 [%]	*Z* [%]
40	69	220	50	82

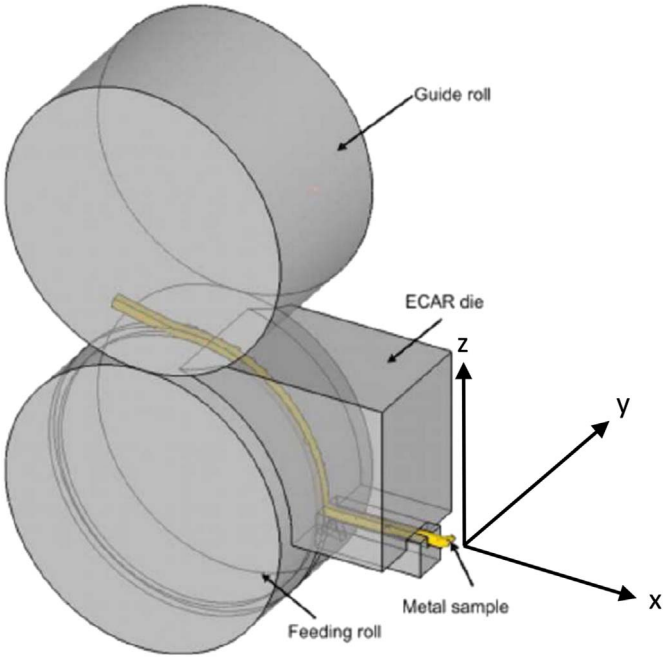

Fig. 1. The schematic of the ECAR facility.

radiation. The Debye–Scherrer diffraction rings were detected by two dimensional imaging plates and the line profiles were determined as the intensity distributions perpendicular to the rings obtained by integrating the two dimensional intensity distributions along the rings. The evaluation of the patterns was carried out by the Convolutional Multiple Whole Profile (CMWP) fitting method [24]. In this procedure, the experimental diffraction pattern is fitted by the sum of a background spline and the convolution of the instrumental pattern and the theoretical line profiles related to crystallite size, dislocations and planar faults. The theoretical line profile functions used in this fitting procedure were based on a model of the microstructure where the crystallites have spherical shape and a log-normal size distribution. As an example, Fig. 2 shows the CMWP fitting for the sample processed by 1 ECAR pass. The following parameters of the microstructure were determined by the CMWP fitting procedure: the area-weighted mean crystallite size ($\langle x \rangle_{area}$), the average dislocation density (ρ) and the dislocation arrangement parameter (*M*). The area-weighted mean crystallite size ($\langle x \rangle_{area}$) was calculated as $\langle x \rangle_{area} = m \cdot \exp(2.5\ \sigma^2)$, where *m* is the median and σ^2 is the log-normal variance of the crystallite size distribution. The value of the parameter *M* reflects the

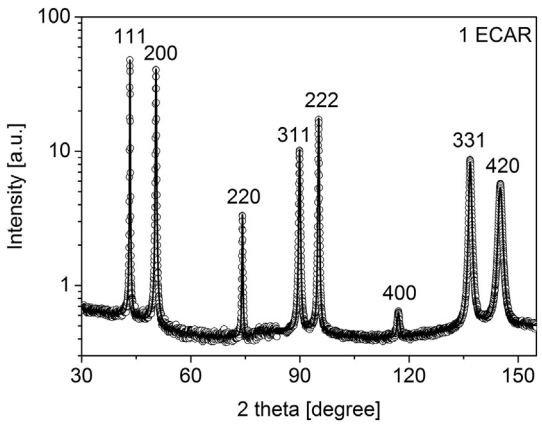

Fig. 2. CMWP fitting for the sample processed by 1 ECAR pass. The open circles and the solid line represent the measured and the fitted X-ray diffraction patterns. The intensity is shown in logarithmic scale.

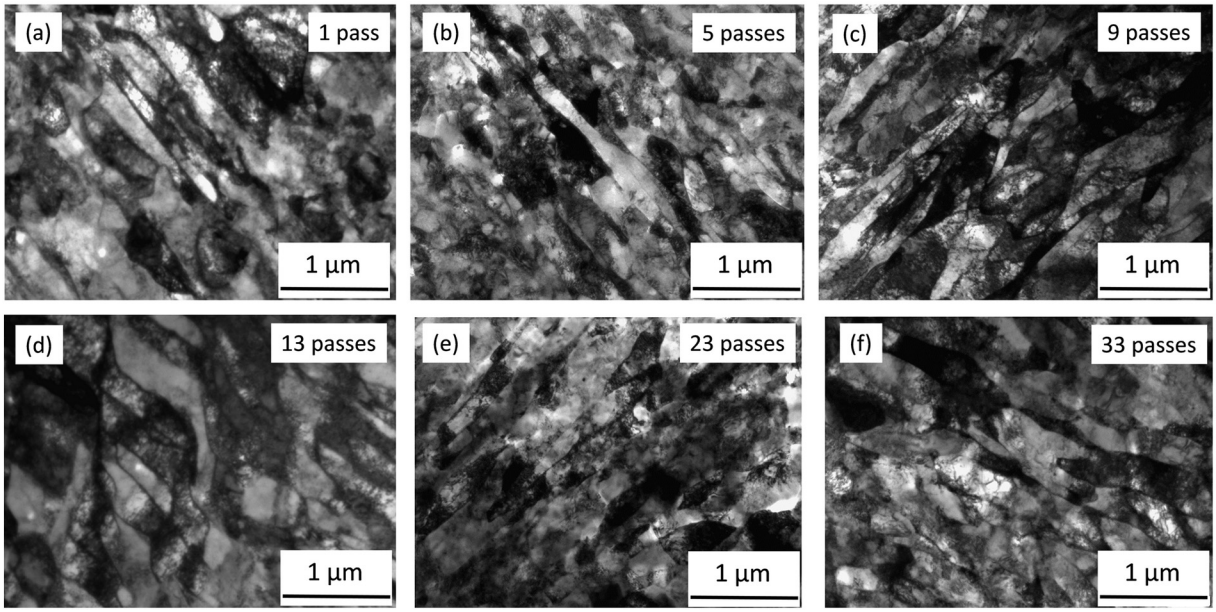

Fig. 3. TEM images showing the microstructures for the samples processed by 1, 5, 9, 13, 23 and 33 passes of ECAR.

arrangement of the dislocations. Thus, a smaller value of *M* relates to a more shielded strain field of the dislocations and the arrangement of dislocations into low energy configurations, such as LAGBs or dipoles, yields a consequent decrease in *M*.

The mechanical properties of the ECAR-processed specimens was studied by uniaxial static tensile test at RT using Tinius Olsen machine. The diameter of the circular cross-sections of the tensile specimens was ~4 mm, therefore the initial cross-sectional area was ~12.6 mm^2. The length of the initial samples was ~10 mm. The strain rate during tension was 0.01 s^{-1}. The energy stored in the ECAR-processed samples was measured by differential scanning calorimetry (DSC) using a Netzsch STA 449 F3 Jupiter calorimeter at a heating rate of 30 K/min.

3. Results

3.1. Characterization of the Microstructure Evolution as a Function of Numbers of ECAR Passes

The TEM images in Fig. 3 show the microstructures in the samples processed by 1, 5, 9, 13, 23 and 33 passes. It can be seen that an UFG microstructure was developed even after the 1st pass of ECAR. Many elongated grains can be seen in Fig. 3a in accordance with the rolling step and the application of route A in ECAR-processing. The horizontal direction in the TEM images is parallel to axis *x* in Fig. 1 which is referred to as longitudinal direction. The vertical direction in the TEM images is parallel to axis *z* in Fig. 1 and referred to as transverse direction. Fig. 4 shows the evolution of the average grain size as a function of the number of ECAR passes which was obtained from the TEM images. The grain size was determined from the bright field TEM images shown in Fig. 3. Only those areas in the micrographs were identified as grains which exhibited strongly different contrast compared to the neighboring regions. Despite this careful evaluation of the TEM images, the inclusion of some subgrains in the group of the identified grains cannot be excluded. For low numbers of ECAR passes, the length and the thickness of the grains with elongated shape were determined individually. Then, the average of these values was considered as the grain size and the ratio of the length and the thickness gave the aspect ratio. About 20 grains were evaluated for each sample and their grain sizes and aspect ratios were averaged and plotted in Fig. 4. The grain size was refined from about 40 µm to ~1.3 µm even after 1 pass of ECAR. Due to the elongated grain size, the average aspect

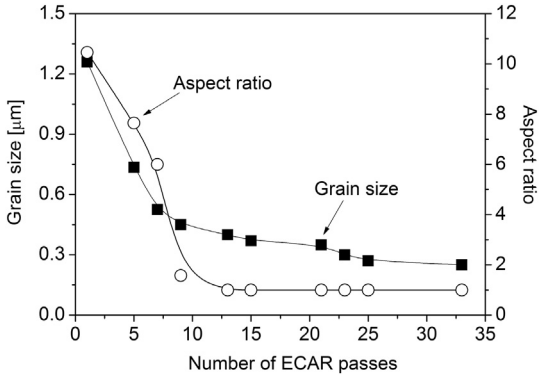

Fig. 4. The average grain size and the grain aspect ratio as a function of the number of ECAR passes.

ratio of the grains was about 10. Between 1 and 7 passes, the grain size decreased quickly to ~500 nm. Then, further increase of the number of passes yielded only a slow reduction in the grain size. The minimum grain size achieved after 33 passes was ~250 nm. Comparing the TEM images in Fig. 3a–f, it is revealed that the grain shape became more equiaxed with increasing the number of passes. This trend was quantified by the decreasing grain aspect ratio in Fig. 4. After 13 passes, the aspect ratio was close to one and accordingly elongated grains were only rarely observed in the TEM images (see Fig. 3e and f).

Fig. 5a shows the evolution of the crystallite size and the dislocation density determined by XLPA as a function of the number of ECAR passes. The crystallite size was ~80 nm after the 1st pass of ECAR and this value did not change significantly with increasing the number of passes. It is noted that the crystallite size determined by XLPA was smaller than the grain size obtained by TEM. This difference is due to the hierarchical microstructure in SPD-processed metals where the grains bounded by high-angle grain boundaries are subdivided into subgrains and/or dislocation cells which scatter X-rays incoherently [25]. Therefore, the crystallite size measured by XLPA is equivalent to the size of subgrains and dislocation cells and its value is smaller than the grain size in SPD-processed materials. Former studies have shown (e.g., [26]) that these subgrains are rather equiaxed even if the grains are elongated.

A high dislocation density (~11 × 10^{14} m^{-2}) was developed in the

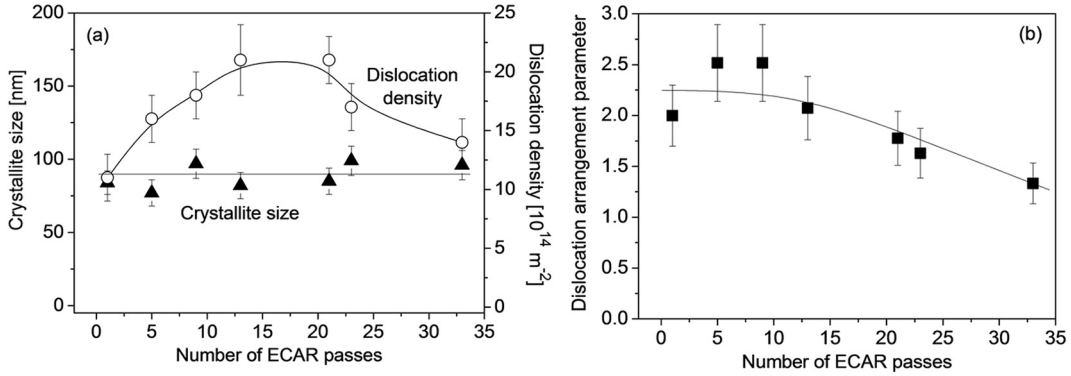

Fig. 5. The crystallite size and the dislocation density (a) as well as the dislocation arrangement parameter (b) as a function of the number of ECAR passes.

OFHC Cu material even after the first pass of ECAR as shown in Fig. 5a. The dislocation density increased with increasing the number of ECAR passes and saturated at the value of $\sim 21 \times 10^{14}\ m^{-2}$ after 13 passes. Between the 21st and the 33rd ECAR passes, the dislocation density was reduced to $\sim 14 \times 10^{14}\ m^{-2}$ which can be attributed to a structural relaxation including annihilation of extrinsic dislocations. These dislocations are not necessary geometrically for the accommodation of lattice misorientations across grain/subgrain boundaries. Similar reduction of the dislocation density has also been observed for Cu processed by ECAP at RT [22,23]. In addition to the change of the dislocation density, the dislocation arrangement parameter also varied during ECAR processing as shown in Fig. 5b. Indeed, for high number of ECAR passes the value of parameter *M* slightly decreased, indicating a stronger shielding of the strain field of dislocations. This observation is in accordance with the occurrence of a structural relaxation for high numbers of ECAR passes.

It is noted that despite the significant change in the dislocation density with increasing the number of ECAR passes, the crystallite size remained unchanged (see Fig. 5a). The very high dislocation density ($\sim 10^{15}\ m^{-2}$) developed after the first pass of ECAR resulted in a very fine subgrain structure with the crystallite size of ~80 nm. Although, the dislocation density increased by a factor of two between 1 and 23 passes of ECAR, the crystallite size remained unchanged, suggesting that the additionally formed dislocations were accumulated at the preexisting subgrain and grain boundaries. Therefore, the misorientations between the neighboring subgrains increased, resulting in a grain refinement due to the increased fraction of high-angle grain boundaries. Between 23 and 33 passes of ECAR, the annihilation of extrinsic dislocations did not yield the change of the grain and subgrain sizes.

3.2. Calorimetry Study of the ECAR-processed Samples

The present DSC experiments revealed the development of an exothermic peak for each sample which is related to the recovery and the recrystallization of the UFG microstructure in the ECAR-processed OFHC Cu. The tempearture of the peak maximum and the area under the peak (i.e., the released heat) were determined and plotted as a function of the number of ECAR passes in Fig. 6. There is a large reduction in the temperature of the peak maximum between 1 and 5 passes, and then it decreases only slightly between 5 and 13 passes. The lowest value of the peak temperature was ~493 K. This value corresponds to a homologous temperature of ~0.36. Between 25 and 33 passes, a moderate increase of the peak temperature to ~515 K was detected. The released heat also increased strongly between 1 and 5 passes and reached a value of about 0.8 J/g. Only a slight increase to ~0.9 J/g was observed during further straining up to 9 passes. Lower values of the released heat (about 0.7 J/g) were detected for 13 and 33 passes. This reduction of the stored energy can be explained by structural relaxation as it will be discussed in Section 4.

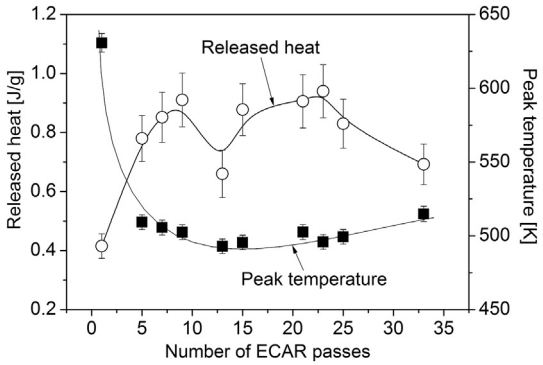

Fig. 6. The released heat and the peak maximum temperature measured by DSC as a function of the number of ECAR passes.

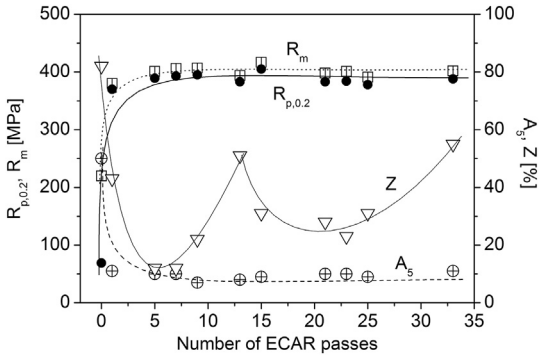

Fig. 7. The proof stress ($R_{p0.2}$), the tensile strength (R_m), the elongation to failure (A_5) and the reduction in area during tension (Z) as a function of the number of ECAR passes.

3.3. Changes in the Mechanical Properties During ECAR

The proof stress ($R_{p0.2}$), the tensile strength (R_m), the elongation to failure (A_5) and the reduction in area during tension (Z) as a function of the number of ECAR passes are shown in Fig. 7. The reduction of the cross sectional area of the specimen measures the contraction of the sample during tension. The proof stress increased from ~69 to ~370 MPa while the tensile strength rised from ~220 to ~380 MPa even after the first pass of ECAR. Further ECAR passes yielded only a slight increase in both the proof stress and the tensile strength. The maximum values of $R_{p0.2}$ and R_m were about 400 and 410 MPa, respectively. Concerning the ductility of the ECAR-processed samples, the elongation to failure decreased from ~50 to ~10% immediately after the first pass. Similarly, the reduction in area during tension was reduced from ~82 to ~43% during the first ECAR pass. Additional ECAR deformation did not result in a considerable change in the elongation to failure. At the same time, the reduction in area further decreased to

~12% after 5 passes of ECAR. Fig. 7 shows that significant improvement in Z to about 50% occurred for 13 and 33 passes. The increase of the reduction in area without the improvement of the elongation to failure indicates an increase of strain localization. The possible reasons of this effect will be discussed in Section 4.

4. Discussion

4.1. ECAR Versus ECAP

Among the SPD procedures, ECAP is the most frequently used method for producing bulk UFG materials. Therefore, it is worth to make a comparison between the microstructures, mechanical properties and thermal stability of Cu processed by the present ECAR procedure and the available literature data obtained on ECAP-processed Cu. It has been shown that the maximum dislocation density in 99.98% purity Cu processed by ECAP was $\sim 21 \times 10^{14}\ m^{-2}$ [4,23] which agrees well with the value obtained by ECAR. In addition, the saturation grain and crystallite sizes in ECAP-processed Cu were ~200 and ~70 nm, respectively [4], which are close to the values determined for ECAR (~250 and ~80 nm, respectively). The similar microstructures for ECAR and ECAP yielded similar mechanical behavior. The proof stress and the elongation to failure in the saturation state of the ECAP-processed Cu were ~400 MPa and ~11% [4,22,23,27,28] which are the same as the values obtained after ECAR (see Section 3.3). In addition, for large number of ECAP passes (N = 15 or more), a decrease of the dislocation density to about $\sim 15 \times 10^{14}\ m^{-2}$ was detected, which is very similar to the observed structural relaxation between the 21st and 33rd passes for the present ECAR-processed samples. Regarding the thermal stability of the UFG microstructure, the heat released in the DSC experiment and the exothermic peak temperature obtained for the saturation state of the present ECAR-processed Cu (~493 K and ~0.9 J/g) were also in good agreement with the values determined for ECAP. In the case of ECAP, the DSC peak temperatures reported in the literature varied between 470 and 530 K at a heating rate of 40 K/min, while the released heat was around ~1.0 J/g [29,30]. It can be concluded that both the microstructure and the properties of ECAR-processed Cu are similar to those obtained for ECAP. At the same time, ECAR is capable for the mass production of UFG metallic materials with high strength. Therefore, ECAR is a possible way of commercialization of SPD-processed metallic materials.

4.2. Comparison Between the Measured and the Calculated Stored Energies

Former experiments [4,31,32] have shown that the heat released during DSC experiments (H) can be considered as the sum of the energies stored in dislocations (E_{disl}), grain boundaries (E_{GB}) and vacancies/vacancy clusters (E_{vac}):

$$H = E_{disl} + E_{GB} + E_{vac}. \quad (1)$$

The contribution of dislocations to the stored energy can be expressed as [4]:

$$E_{disl} = A\frac{Gb^2\rho}{\rho_m}\ln\frac{R_e}{b}, \quad (2)$$

where G is the shear modulus (47 GPa for Cu), b is the magnitude of Burgers vector (0.25 nm for Cu), ρ is the dislocation density, R_e is the outer cut-off radius of dislocations (also obtained by XLPA), ρ_m is the mass density ($8.96 \times 10^6\ g^{-3}$ for Cu) and A stands for the factor depending on the edge/screw character of dislocations. The value of A equals to $(4\pi)^{-1}$ and $(4\pi(1-\nu))^{-1}$ for screw and edge dislocations, respectively, where ν is the Poisson's ratio (0.3 was taken). The parameter q determined from XLPA describes the edge/screw character of dislocations. The theoretically calculated values of q for pure edge and screw dislocations in Cu are 1.68 and 2.37, respectively [25]. In the case of mixed dislocations the value of A can be obtained from the experimentally determined q using a simple rule of mixture:

$$A = \frac{q-1.68}{0.69}\frac{1}{4\pi} + \frac{2.37-q}{0.69}\frac{1}{4\pi(1-\nu)}. \quad (3)$$

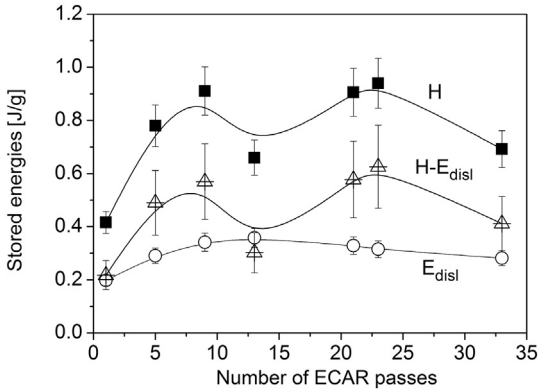

Fig. 8. The released heat measured by DSC (H), the calculated energy stored in dislocations (E_{disl}) and their difference as a function of the number of ECAR passes.

The energy stored in dislocations was calculated from Eqs. (2) and (3) and plotted as a function of the number of ECAR passes in Fig. 8. The calculation was carried out only for those numbers of passes for which the dislocation density was determined. The value of E_{disl} was ~0.2 J/g after the first pass of ECAR which increased to ~0.36 J/g in the saturation state (after 13 passes). Further deformation up to 33 passes resulted in a reduction of the energy stored in dislocations to ~0.28 J/g. It can be concluded that the contribution of dislocations to the stored energy is about one-third of the heat released during DSC. This observation is in agreement with former results obtained on ECAP-processed face-centered cubic UFG metals [4].

The difference between the measured released heat (H) and the calculated E_{disl} can be related to the energy stored in grain boundaries and/or vacancies. It is noted that the energy of low-angle grain boundaries (LAGBs) was included in E_{disl} as LAGBs are usually built up from dislocations. Therefore, the difference between H and E_{disl} includes only the energy of high-angle grain boundaries (HAGBs), in addition to the energy stored in vacancies. Fig. 8 shows that the quantity H-E_{disl} follows a non-monotonous trend and its value decreases at 13 and 33 passes. The relatively low values of H-E_{disl} can be caused by the reduction of the specific energy of HAGBs, the decrease of the HAGB fraction and/or the reduction of the vacancy concentration. As the grain refinement during SPD usually occurs by the development of HAGBs from LAGBs [4,33,34], therefore the decrease of HAGB fraction with increasing the number of ECAR passes is not expected. At the same time, a dynamic relaxation of grain boundaries causing reduction of the specific HAGB energy and/or the annihilation of vacancies inside the grains may occur during severe deformation of UFG microstructures [4]. Indeed, former studies [35–37] have shown that the excess vacancy concentration might achieve a value of 10^{-4} in SPD-processed metals which is about 17 orders of magnitude higher than the equilibrium value. In addition, the grain boundaries are in a non-equilibrium state, which means that their energy is higher than the minimum energy required for a boundary with the same misorientation. The higher grain boundary energy may be caused by the excess dislocations and vacancies accumulated along the HAGBs.

Fig. 8 suggests that the stored energy increased with increasing the number of ECAR passes and achieved a value of about 0.9 J/g after 9 passes. The majority of this stored energy (about two-third) is related to vacancies and HAGBs. This high stored energy is the driving force for vacancy annihilation and/or grain boundary relaxation occurred between 9 and 13 passes of ECAR. As a result of this dynamic relaxation, the energy stored in vacancies and/or HAGBs decreased from ~0.6 J/g to ~0.3 J/g. Continuing deformation after 13 passes, the vacancy

concentration increased again and for 23 passes the stored energy achieved a similar value (~0.9 J/g) as before the first relaxation process between 9 and 13 passes. Then, between 23 and 33 passes a vacancy annihilation and a grain boundary relaxation occurred which is also complemented by the decrease of the dislocation density (see Fig. 8). It is worth to note that in the first structural relaxation process between 9 and 13 passes the dislocation did not changed significantly while between 21 and 33 passes a considerable decrease in the dislocation density was observed. This difference between the two relaxation processes can be attributed to the different arrangement of dislocations. For 21 passes, the dislocation structure was more clustered than for 9 passes as indicated by the smaller dislocation arrangement parameter for the former case (see Fig. 5b). The dislocation annihilation is faster in a more clustered arrangement due to the smaller spacing between the individual dislocations.

4.3. Correlation Between the Microstructure and the Mechanical Properties of ECAR Processed Cu

Former studies [4,23] on ECAP-processed Cu revealed that the yield strength can be related to the dislocation density using the well-known Taylor equation:

$$\sigma_{Taylor} = \sigma_0 + \alpha M^T G b \rho^{1/2}, \quad (4)$$

where σ_0 is a threshold stress (~35 MPa for Cu [23]), α is a constant describing the dislocation strengthening and M^T is the Taylor factor. The samples investigated in this study did not exhibit a strong texture and therefore M^T was taken as 3.06. The formerly published good correlation between the measured yield strength and the values calculated from Eq. (4) suggests that in SPD-processed pure fcc metals dislocations give the main contribution to the strength which can be expressed solely by the dislocation density using Eq. (4) without an additive Hall-Petch term. This observation can be explained by the fact that the dislocation density determined by XLPA includes all dislocations located either at the boundaries or in the grain interiors. In SPD-processed microstructures, many dislocations are accumulated at the HAGBs through pile ups and therefore gliding dislocations interact with these dislocations rather than directly with the grain boundaries. As a consequence, HAGB hardening is practically included in Eq. (4) and α may be regarded as an effective dislocation strengthening parameter. For Cu processed by ECAP between 1 and 25 passes, the value of α was found to be 0.25 ± 0.04 [23]. In the present study, α was calculated for the different numbers of ECAR passes from the measured dislocation density and proof stress values using Eq. (4). This calculation showed that parameter α varies between 0.21 and 0.27 for the different numbers of ECAR passes, therefore it is in good agreement with the values obtained formerly for ECAP-processed Cu (see above). It is noted that the value of α depends on the arrangement of dislocations, therefore it slightly changed with increasing the number of ECAR passes. For instance, between 23 and 33 passes parameter α increased from 0.21 to 0.26 which can be explained by the arrangement of dislocations into a low energy configuration, in accordance with the decrease of parameter M determined by XLPA (see Fig. 5a). Former studies have shown that the value of α varies between 0.1 and 0.4 [23] and a less clustered dislocation structure is associated with a lower value of α [38]. The increase of the value of α between 23 and 33 passes compensated the reduction of the dislocation density, thereby the yield strength remained unchanged for high numbers of ECAR passes.

The defect structure relaxation observed by DSC for 13 and 33 passes of ECAR did not cause significant change in the proof stress, tensile strength and elongation to failure. At the same time, for these passes the reduction in area (Z) increased considerably as shown in Fig. 7. The higher value of Z without the improvement of A_5 suggests a stronger strain localization during tensile testing. This means that the resistance of the samples against necking decreased for 13 and 33 passes of ECAR. Our experimental results suggest a considerable vacancy annihilation inside the grains and/or grain boundary relaxation for these passes. The latter effect can make the deformation mechanisms at the grain boundaries (such as grain boundary sliding) more difficult due to the slower diffusion along the boundaries. The decreased role of the deformation mechanisms at the grain boundaries might reduce the strain rate sensitivity which yielded an easier necking during tension for 13 and 33 passes of ECAR. At the same time, the much lower vacancy concentration inside the grains might result in a more difficult formation of voids during tension, therefore the material exhibited improved resistance against fracture in the neck. Thus, despite the strong strain localization, the elongation to failure did not decrease for 13 and 33 passes of ECAR (see Fig. 7).

5. Summary and Conclusions

OFHC copper was processed by ECAR up to 33 passes at RT. The microstructure and the mechanical properties were studied as a function of number of ECAR passes using TEM, XLPA, DSC and tensile testing. The following conclusions have been drawn:

1. A non-monotonous evolution of the dislocation density with increasing number of ECAR passes was observed. First, the dislocation density increased with increasing number of ECAR passes and saturated at the value of $\sim 21 \times 10^{14}\ m^{-2}$ after 13 passes. Between 21 and 33 passes the dislocation density was reduced to $\sim 14 \times 10^{14}\ m^{-2}$. The decrease of the dislocation density for high numbers of passes was accompanied by the rearrangement of dislocations into low energy configurations as indicated by the decrease of the dislocation arrangement parameter determined by XLPA.
2. The variation of the heat released during DSC annealing was also non-monotonous as a function of the number of ECAR passes. First, the released heat increased with increasing the number of ECAR passes and saturated at the value of ~0.9 J/g after 9 passes. For 13 and 33 passes of ECAR, the released heat decreased by about 30% as compared to its saturation value which can be attributed to the decrease of the vacancy concentration and/or grain boundary relaxation.
3. The proof stress and the ultimate tensile strength saturated at a value of about 400 MPa after 5 passes of ECAR. The proof stress was successfully related to the dislocation density using the Taylor equation which indicates that dislocations give the major contribution to the strength. The reduction in area during tension was improved after 13 and 33 passes which suggests stronger strain localization in these samples. This effect might be caused by the relaxation of the grain boundaries and the annihilation of vacancies inside the grains.
4. The minimum grain size, the maximum dislocation density as well as the saturation values of the strength and ductility achieved by ECAR at RT were similar to the values obtained formerly for ECAP-processed Cu. This is also valid for the released heat and the exothermic peak temperature determined by DSC. At the same time, ECAR is capable for the mass production of UFG metallic materials with high strength. Therefore, ECAR may be a possible way of commercialization of SPD-processed Cu.

Acknowledgements

This work was performed within the frame of the project “Technological preparation of electrotechnical steels with high permeability for electrodrives with higher efficiency” which is supported by the Operational Program “Research and Development” ITMS 26220220037, financed through European Regional Development Fund and the VEGA 1/0325/14 project. This research was also supported by the Hungarian Scientific Research Fund (OTKA), Grant nos. K109021

and PD121049.

References

[1] V.M. Segal, Materials processing by simple shear, Mater. Sci. Eng. A 197 (1995) 157–164.
[2] R.Z. Valiev, R.K. Islamgaliev, I.V. Alexandrov, Bulk nanostructured materials from severe plastic deformation, Prog. Mater. Sci. 45 (2000) 103–189.
[3] Y. Saito, H. Utsunomiya, N. Tsuji, T. Sakai, Novel ultra-high straining process for bulk materials - development of the accumulative roll-bonding (ARB), Acta Mater. 47 (1999) 579–583.
[4] J. Gubicza, Defect Structure and Properties of Nanomaterials, 2nd and Extended Edition, Woodhead Publishing, Duxford, UK, 2017 (an imprint of Elsevier).
[5] R.Z. Valiev, T.G. Langdon, Principles of equal channel angular pressing as a processing tool for grain refinement, Prog. Mater. Sci. 51 (2006) 881–981.
[6] R.Z. Valiev, Y. Estrin, Z. Horita, T.G. Langdon, M. Zehetbauer, Y.T. Zhu, Producing bulk ultrafine-grained materials by severe plastic deformation, J. Miner. Met. Mater. Soc. 58 (4) (2006) 33–39.
[7] Y. Iwahashi, J. Wang, Z. Horita, M. Nemoto, T.G. Langdon, Principle of equal-channel angular pressing for the processing of ultra-fine grained materials, Scr. Mater. 35 (1996) 143–146.
[8] K. Nakashima, Z. Horita, M. Nemoto, T.G. Langdon, Development of a multi-pass facility for equal-channel angular pressing to high total strains, Mater. Sci. Eng. A 281 (2000) 82–87.
[9] A.P. Zhilyaev, T.G. Langdon, Using high-pressure torsion for metal processing: fundamentals and applications, Prog. Mater. Sci. 53 (2008) 893–979.
[10] Y. Nakao, H. Miura, Nano-grain evolution in austenitic stainless steel during multi-directional forging, Mater. Sci. Eng. A 528 (2011) 1310–1317.
[11] Y. Beygelzimer, D. Orlov, V. Varyukhin, A new severe plastic deformation method: twist extrusion, in: Y.T. Zhu, T.G. Langdon, R.S. Mishra, S.L. Semiatin, M.J. Saran, T.C. Lowe (Eds.), Ultrafine Grained Materials II, TMS (The Minerals, Metals and Materials Society), 2002, pp. 297–304.
[12] J.-H. Han, H.-K. Seok, Y.-H. Chung, M.-C. Shin, J.-C. Lee, Texture evolution of the strip cast 1050 Al alloy processed by continuous confined strip shearing and its formability evaluation, Mater. Sci. Eng. A 323 (2002) 342–347.
[13] T. Kvackaj, A. Kovacova, M. Kvackaj, R. Kocisko, L. Litynska-Dobrzynska, V. Stoyka, M. Miháliková, TEM studies of structure in OFHC copper processed by equal channel angular rolling, Micron 43 (2012) 720–724.
[14] A. Habibi, M. Ketabchi, Enhanced properties of nano-grained pure copper by equal channel angular rolling and post-annealing, Mater. Des. 34 (2012) 483–487.
[15] M. Mahmoodi, M. Sedighi, D.A. Tanner, Investigation of through thickness residual stress distribution in equal channel angular rolled Al 5083 alloy by layer removal technique and X-ray diffraction, Mater. Des. 40 (2012) 516–520.
[16] A. Azimi, S. Tutunchilar, G. Faraji, M.K. Besharati Givi, Mechanical properties and microstructural evolution during multi-pass ECAR of Al 1100–O alloy, Mater. Des. 42 (2012) 388–394.
[17] C.Y. Nam, J.H. Han, Y.H. Chung, M.C. Shin, Effect of precipitates on microstructural evolution of 7050 Al alloy sheet during equal channel angular rolling, Mater. Sci. Eng. A 347 (2003) 253–257.
[18] Y.Q. Cheng, Z.H. Chen, W.J. Xia, Drawability of AZ31 magnesium alloy sheet produced by equal channel angular rolling at room temperature, Mater. Charact. 58 (2007) 617–622.
[19] Y.Q. Cheng, Z.H. Chen, W.J. Xia, T. Zhou, Effect of channel clearance on crystal orientation development in AZ31 magnesium alloy sheet produced by equal channel angular rolling, J. Mater. Process. Technol. 184 (2007) 97–101.
[20] F.Z. Hassani, M. Ketabchi, Nano grained AZ31 alloy achieved by equal channel angular rolling process, Mater. Sci. Eng. A 528 (2011) 6426–6431.
[21] M. Honarpisheh, M. Dehghani, E. Haghighat, Investigation of mechanical properties of Al/Cu strip produced by equal channel angular rolling, Proc. Mater. Sci. 11 (2015) 1–5.
[22] F. Dalla Torre, R. Lapovok, J. Sandlin, P.F. Thomson, C.H.J. Davies, E.V. Pereloma, Microstructures and properties of copper processed by equal channel angular extrusion for 1–16 passes, Acta Mater. 52 (2004) 4819–4832.
[23] J. Gubicza, N.Q. Chinh, J.L. Lábár, S. Dobatkin, Z. Hegedűs, T.G. Langdon, Correlation between microstructure and mechanical properties of severely deformed metals, J. Alloys Compd. 483 (2009) 271–274.
[24] G. Ribárik, J. Gubicza, T. Ungár, Correlation between strength and microstructure of ball milled Al-Mg alloys determined by X-ray diffraction, Mater. Sci. Eng. A 387–389 (2004) 343–347.
[25] J. Gubicza, X-ray Line Profile Analysis in Materials Science, IGI-Global, Hershey, PA, USA, 2014.
[26] D.A. Hughes, N. Hansen, Microstructure and strength of nickel at large strains, Acta Mater. 48 (2000) 2985–3004.
[27] F.H. Dalla Torre, A.A. Gazder, C.F. Gu, C.H.J. Davies, E.V. Pereloma, Grain size, misorientation, and texture evolution of copper processed by equal channel angular extrusion and the validity of the Hall–Petch relationship, Metall. Mater. Trans. A 38 (2007) 1080–1095.
[28] J. Gubicza, L. Balogh, R.J. Hellmig, Y. Estrin, T. Ungár, Dislocation structure and crystallite size in severely deformed copper by X-ray peak profi le analysis, Mater. Sci. Eng. A 400–401 (2005) 334–338.
[29] J. Gubicza, S.V. Dobatkin, E. Khosravi, A.A. Kuznetsov, J.L. Lábár, Microstructural stability of Cu processed by different routes of severe plastic deformation, Mater. Sci. Eng. A 528 (2011) 1828–1832.
[30] L. Balogh, J. Gubicza, R.J. Hellmig, Y. Estrin, T. Ungár, Thermal stability of the microstructure of severely deformed copper, Z. Kristallogr. (Suppl. 23) (2006) 381–386.
[31] Z. Hegedűs, J. Gubicza, M. Kawasaki, N.Q. Chinh, K. Süvegh, Z. Fogarassy, T.G. Langdon, High temperature thermal stability of ultrafine-grained silver processed by equal-channel angular pressing, J. Mater. Sci. 48 (2013) 1675–1684.
[32] W.Q. Cao, C.F. Gu, E.V. Pereloma, C.H.J. Davies, Stored energy, vacancies and thermal stability of ultrafine grained copper, Mater. Sci. Eng. A 492 (2008) 74–79.
[33] O.V. Mishin, D. Juul Jensen, N. Hansen, Microstructures and boundary populations in materials produced by equal channel angular extrusion, Mater. Sci. Eng. A 342 (2003) 320–328.
[34] S.V. Dobatkin, J.A. Szpunar, A.P. Zhilyaev, J.-Y. Cho, A.A. Kuznetsov, Effect of the route and strain of equal-channel angular pressing on structure and properties of oxygen-free copper, Mater. Sci. Eng. A 462 (2007) 132–138.
[35] D. Setman, E. Schafler, E. Korznikova, M.J. Zehetbauer, The presence and nature of vacancy type defects in nanometals detained by severe plastic deformation, Mater. Sci. Eng. A 493 (2008) 116–122.
[36] J. Cizek, M. Janecek, O. Srba, R. Kuzel, Z. Barnovska, I. Prochazka, S. Dobatkin, Evolution of defects in copper deformed by high-pressure torsion, Acta Mater. 59 (2011) 2322–2329.
[37] E. Schafler, G. Steiner, E. Korznikova, M. Kerber, M.J. Zehetbauer, Lattice defect investigation of ECAP-Cu by means of X-ray line profile analysis, calorimetry and electrical resistometry, Mater. Sci. Eng. A 410–411 (2005) 169–173.
[38] F. Hernandez Olivares, J. Gil Sevillano, A quantitative assessment of forest-hardening in FCC metals, Acta Metall. 35 (1987) 631–641.